J. Indian Inst. Sci.
A Multidisciplinary Reviews Journal
ISSN: 0970-4140 Coden-JIISAD

REVIEW ARTICLE

Phase-field Modeling of Phase Transformations in Multicomponent Alloys: A Review

*Arka Lahiri**

Abstract | Almost all alloys of engineering importance are multicomponent in character. Multicomponent alloys are subject to complex interplay of thermodynamic and kinetic parameters and display a rich variety of microstructural features which are not seen in binary alloys. Achieving microstructural control of multicomponent alloys is central to their efficacy in specific applications. Unraveling the chemistry-thermomechanical processing-microstructure relationships in multicomponent alloys only through experiments have been proven to be a resource intensive approach. Quantitative simulations of microstructural evolution in multicomponent alloys using the technique of phase-field modeling can significantly offset the experimental burden and provide an energy efficient and sustainable framework for alloy design. In this review, we focus on those phase-field models which can consider the evolution of multiple phases simultaneously in a multicomponent system and attempt to understand the history of their emergence as tools of predictive value. We briefly review the studies conducted with such multiphase, multicomponent phase-field models and conclude with a commentary on the future role of phase-field modeling towards the sustainable development of novel multicomponent alloys.

Keywords: *Phase-field, Multicomponent alloy, Multiphase, Microstructure, ICME*

1 Introduction

Material properties are complex functions of their structural hierarchy which span multiple length scales. The most fundamental instance of structure in a material is the crystal structure with the associated length scales of unit cell dimensions, which are of the order of several angstroms (Å). The crystal structure is determined through the interactions of constituent atoms at the level of their electronic clouds and hence is predominantly decided by the material chemistry. Other than optimizing the choice of chemical components and their relative fractions, very little can be done to alter the crystal structure and the associated length scale. Material properties like melting point, elastic moduli, specific heat capacity, etc., are determined by the underlying crystal structures.

In addition to the crystal structure, a material also possesses a microstructure and as the name suggests it exists over length scales ranging from several microns (μm) to several hundred μm and is defined by the distribution of different phases possessing distinct crystal structures and/or compositions. The phase morphologies, volume fractions, and the arrangement of phases relative to each other are the critical parameters which define the microstructures. Additionally, a microstructure can also be made up of grains of the same phase which differ from each other in terms of crystal orientations. In that case, the grain sizes and their orientation distributions become the parameters of importance. In

[1] *Metallurgical and Materials Engineering Department, Indian Institute of Technology Roorkee, Haridwar 247667, Uttarakhand, India.*
**arka.lahiri@mt.iitr.ac.in, arkalahiri2009@gmail.com*

contrast to the material properties determined by crystal structures, properties like strength, ductility, toughness, creep resistance, etc., which are governed by the microstructural states of materials, demonstrate a strong length scale dependence. For example, a finely spaced distribution of second phase precipitates in an alloy usually provides much more effective resistance to dislocation glide and concomitantly leads to a larger improvement in alloy strength in comparison to a coarser distribution. As microstructural length scales can be modified by thermomechanical processing, it offers another avenue to design microstructures in addition to controlling the alloy chemistry.

Pure materials made up of a single chemical component possess properties which are rarely useful in engineering applications. Alloying offers the simplest route to enhance material properties leveraging the synergy of interactions of different atoms with each other. With an increase in the number of chemical components, there is a consequent rise in the thermodynamic complexity of the system with the possibility of multiple phases coexisting with each other. Furthermore, the necessity of employing a diffusivity matrix to encapsulate all the kinetic parameters in a multicomponent alloy is proof of its kinetic complexity. The interplay of thermodynamic and kinetic properties of a multicomponent system allows the emergence of a wide variety of microstructural features in them which have not been reported in binary alloys. Consequently, multicomponent alloys display exciting combinations of properties that are rarely achieved in binary alloys motivating extensive research into their design and development.

Optimization of the alloy chemistry and processing conditions through experiments to achieve the perfect microstructure is an iterative process involving extensive characterization and mechanical testing. Computational material science can relieve some of the experimental burden associated with the design novel alloys with specific chemistry and microstructures. Specifically, the concept of multiscale modeling[23, 24, 98] where the predictions of material behaviour obtained from lower length scale simulations are used as an input for computations at higher length scales appear to be rather well suited for this purpose. This approach has already been formalized into the paradigm of "Integrated Computational Materials Engineering (ICME)"[38, 80] with the objective of designing novel materials computationally. An ICME process chain involves modeling techniques spanning the entire gamut of length scales, starting from ab-initio calculations[51, 88] to bulk scale finite element method (FEM)[44, 108] simulations assuming homogeneous material properties. In between the two extremes of atomistic and bulk macroscopic length scales, lies the microstructural or mesoscopic length scale where the heterogeneity at the level of atomic structure is coarse-grained to obtain a continuum description of the material. The heterogeneity that exists at the mesoscopic scale is due to the presence of different phases and their morphologies which collectively constitute the microstructure of the material. Modeling microstructures and predicting key microstructural length scales have driven the emergence of the technique of Phase-field modeling which is the focus of this review.

The basic idea of a phase-field (henceforth called PF) model is to digitize a microstructure by representing the distribution of different phases by their corresponding scalar fields called "order parameters", usually denoted by $\phi(\boldsymbol{x}, t)$. Another name for the order parameter is the "Phase-field" which lends the technique its name. Order parameter fields can be derived by coarse-graining a material property from lower length scales followed by an appropriate normalization scheme. This represents a bottom-up approach of constructing PF models, an example of which is given in Fig. 1a where the order parameter represents normalized solute mole fractions in an alloy. Being conserved over the system, solute mole fractions belong to the class of conserved order parameters. As indicated in Fig. 1a, usually the order parameters are normalized such that $\phi = 1$ indicates the presence while $\phi = 0$ indicates the absence of the corresponding phase. The order parameter fields corresponding to every phase recreates the PF version of the microstructure of the system. In a two-phase microstructure, it is often convenient to associate the presence and absence of either phase with the values $\phi = 1, 0$ of a single order parameter field as shown in Fig. 1. The transition from $\phi = 0$ to $\phi = 1$ happens over a finite width marking a diffuse interface between the phases (see Fig. 1b). It must be remarked that in a PF model derived from a bottom-up approach, the interface width is equal to the experimentally observed physical interface width in the material. Updating the ϕ fields by solving for its governing differential equation results in a simulation of phase transformation.

The bottom-up approach is not the only way to construct a PF model. As the widths of the interfacial region observed experimentally are negligibly small compared to the spatial extent

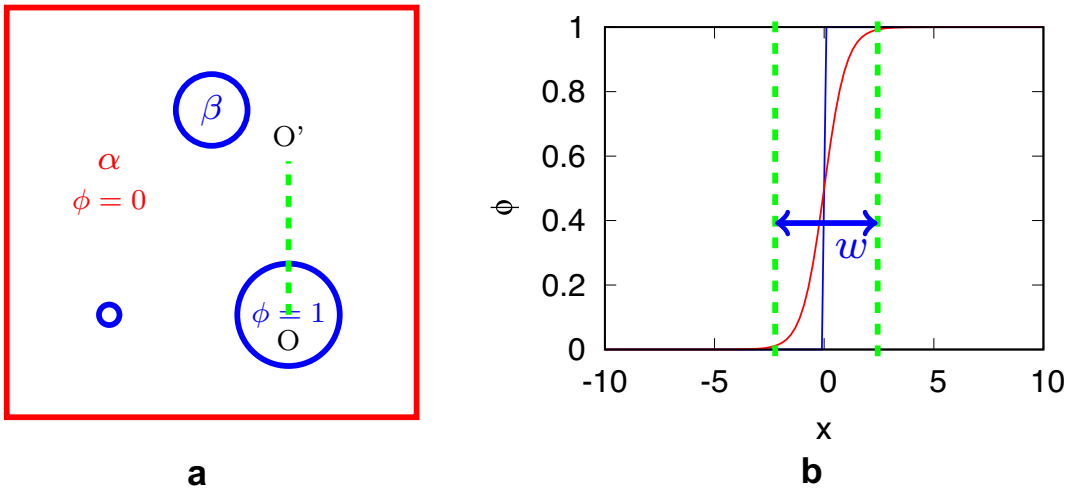

Figure 1: **a** Schematic of a two-phase microstructure with β precipitates embedded in α matrix in a binary alloy. The conserved order parameter ϕ is related to the solute mole fraction field (c) as $\phi = \frac{c - c^{\alpha}}{c^{\beta} - c^{\alpha}}$, where $c^{\alpha,\beta}$ denote the equilibrium compositions of the α and β phases. Consequently, α phase is identified by $\phi = 0$ and the β phase by $\phi = 1$. **b** Schematic of the diffuse interface (red) having width (W) along the OO' axis in (**a**). A sharp interface (blue) is added for reference.

of the phases they separate, it is reasonable to approximate the interfaces by a single plane. Under this approximation, all problems of phase transformation can be treated as "free/moving boundary problems" where the redistribution of solute or latent heat (or any other quantity specific to the problem) at the moving interface provides a boundary condition to the differential equation describing transformation kinetics. A PF model can also be viewed as a diffuse interface model which reduces to the corresponding free boundary problem at the limit of vanishing interface thickness. This is the top-down approach where there is no physical meaning associated with the order parameters and they are just introduced as mathematical functions indicating the distribution of different phases in the microstructure. An example could be the non-conserved order parameter ϕ where $\phi = 0$ represents the liquid phase and $\phi = 1$ represents the solid phase in a PF model of single-phase solidification.

At this stage, it is important to develop an appreciation of the efficacy of diffuse interfaces employed in the PF model. The phase topologies appearing in a microstructure can be quite complex and simulating their evolution using sharp interface models which require explicit tracking of the interfaces is computationally infeasible. PF models in this regard offer an elegant solution by considering the interfaces to be diffuse. Mathematically, such interfaces are marked by smooth, continuous transitions from $\phi = 0$ to $\phi = 1$. Thus, the order parameter fields which represent a PF version of the microstructure are continuous and differentiable throughout. This allows the governing differential equation of order parameter evolution to be solved everywhere in the domain obviating the need for explicit interface tracking. The diffuseness of the interface being principal to the PF model, it needs to be adequately resolved, thus determining the maximum spacing of the numerical grid to be used in a computer simulation. As a wider interface allows a larger domain to be simulated using an identical number of grid points, there is a clear advantage with the top-down approach as it offers the additional flexibility of choosing an artificially large interface width compared to that in a bottom-up approach where the interface width is a physical quantity seen experimentally.

The PF models initially developed for studying transformations in pure materials and binary alloys have finally evolved into a stage where it can tackle transformations involving an arbitrary number of phases in generic multicomponent alloys. In this review, our focus will be on the last category of models and the studies that have been conducted using them. Our review is structured in the following way. First, we trace all the key developments of PF modeling which have empowered it to be used for quantitative predictions. We then follow it up with brief reviews of the key models of multiphase, multicomponent systems, and conclude.

2 Key Developments of the PF Model Prior to the Advent of Generic Multiphase, Multicomponent Models

In view of the pre-existing excellent reviews of PF modeling[5, 16, 71, 74, 75, 77, 89–91], our review of this topic is intentionally succinct and just points to the seminal papers of the field.

Cahn and Hilliard[11, 12] developed the earliest diffuse interface model by treating the free energy of a material system as a non-local function of the solute concentration. Their formulation could self consistently retrieve the interfacial energy and width of any diffuse interface seen experimentally for a particular choice of the simulation parameters. The governing differential equation of order parameter evolution is derived out of a variational energy minimization scheme which conserves solutes[11]. This model has come to be known as the Cahn–Hilliard (henceforth CH) model and has been widely used to simulate solid-state phase transformation in materials[42, 66, 107].

There has been an alternate line of development of PF modeling with the objective of simulating solidification. In contrast to the Cahn-Hilliard model, the order parameters in the PF models of solidification are just introduced for a digital description of the microstructure and are not related to any physical quantity as per the top-down modeling approach. The earliest instance of a PF model derived to model solidification in pure materials is due to Langer[69], followed by models due to Collins, Levine[22] and Kobayashi[58]. Penrose, Fife[81] and Wang et al.[100] presented thermodynamically consistent derivations of evolution equations of order parameters and temperature fields starting from an entropy functional of the system. Moving on to PF modeling of alloys, Wheeler et al.[103] developed a PF model for isothermal solidification in binary alloys where the solid and the liquid phases share the same composition which resulted in an unwanted contribution stemming from the bulk chemical energy to the interfacial energy[56]. This problem is mitigated by introducing separate composition fields for both the solid and the liquid phases which are related to each other through a partition coefficient[99] or through the condition of local equilibrium necessitating equalities of diffusion potentials in both phases[57]. Equalities of diffusion potentials have also been enforced for every two-phase equilibrium in a multiphase PF model of solidification in binary alloys[30, 31].

There are other important developments which have significantly improved the quantitative accuracy of PF models. Parameters appearing in the PF model are related to physical parameters of the free boundary problem through matched asymptotic expansions. For the PF model to replicate the experimental reality of diffusion controlled growth at low driving forces, asymptotics require the PF interface mobility to be extremely high, which results in a numerically stiff differential equation governing order parameter evolution. Karma and Rappel[49, 50] showed that instead of the sharp interface limit, if the PF model is allowed to replicate the properties of the free boundary problem at a thin interface limit, a combination of model parameters exists which allows complete diffusion control at the interface without introducing significant numerical challenges. Thus, the development of the thin interface asymptotics is a crucial step towards realizing quantitatively accurate simulations which are computationally accessible at the same time.

Anomalous solute trapping at a diffuse interface is another issue which limited the quantitative utility of PF models. The interface width in a PF model derived from a top-down approach is an artificial parameter scaled to ensure computational accessibility of large systems. This artificially scaled interface, when separating phases with large differences in solute diffusivity, lead to solute trapping for interface velocities far lower than those observed experimentally. In a PF simulation, solute trapping manifests as a discontinuity between the extrapolated asymptotes of diffusion potentials from either side of the interface. It is mitigated by introducing a non-variational anti-trapping mass flux into the solute diffusion equation to negate the mass flux due to jumps in diffusion potentials at the interface[27, 48].

We have now reviewed some of the key developments concerning PF modeling of phase transformations in binary alloys and pure materials. More complete discussions can be found in the review papers mentioned at the beginning of the section. In the next section, we will describe some of the basic features associated with a PF model. This will help set up the context for the more complicated and generic models discussed later.

3 Basic Structure of a PF Model

The popular multiphase, multicomponent PF models are largely based on a top-down approach where the order parameters serve as indicator functions describing the distribution of different phases in the microstructure. The fundamental structure of such a PF model involves an expression of the total free energy of the system as,

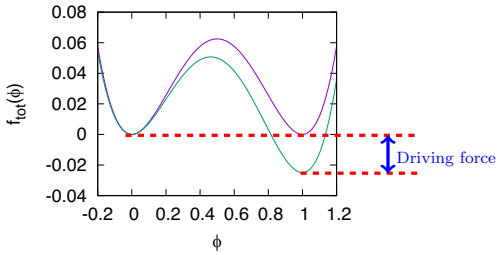

Figure 2: A schematic of $f_{\text{tot}}(\phi) = f_{\text{b}}(\phi) + \left\{(1-h(\phi))f^*_{\phi=0} + h(\phi)f^*_{\phi=1}\right\}$. The purple curve corresponds to the situation where $f^*_{\phi=0} = f^*_{\phi=1} = 0$ and the phases are in equilibrium. The green curve corresponds to a situation where $f^*_{\phi=1} < f^*_{\phi=0} = 0$ and $\phi = 1$ is the equilibrium phase.

$$F = \int_{\Omega} \left[f_{\text{b}}(\phi) + \frac{\kappa}{2}(\nabla\phi)^2 + \left\{(1-h(\phi))f^*_{\phi=0} + h(\phi)f^*_{\phi=1}\right\}\right] \mathrm{d}\Omega, \tag{1}$$

where the integral is over the system volume denoted by Ω and an example of which can be the microstructure in Fig. 1a. The first term on the RHS indicates the bulk-free density $f_{\text{b}}(\phi)$ which is a function of the local value of the phase-field (ϕ) at any point in the microstructure. The purpose of this term is to penalize the non-equilibrium material appearing over the diffuse interfaces, $0 < \phi < 1$ (see Fig. 2). A possible choice of the bulk energy density function known as the double well -potential given by $f_b(\phi) = H\phi^2(1-\phi)^2$ is presented in Fig. 2. The parameter H controls the height of the energy barrier between the equilibrium phases $\phi = 0$ and $\phi = 1$. The second term in Eq. 1 is the gradient energy density term which imposes an energy penalty on gradients in ϕ where κ controls the magnitude of the penalty. This term is a non-local function of ϕ in contrast to $f_{\text{b}}(\phi)$. The bulk energy density gets minimized for a sharp interface while the gradient energy density prefers to have the interface as diffuse as possible. These two terms combine to equilibrate a diffuse interface with a finite width (W) as highlighted in Fig. 1b. The final term delimited by curly braces in Eq. 1 is given by an interpolation of free energy densities of the pure phases ($f^*_{\phi=1}$ and $f^*_{\phi=0}$) which can be due to either of chemical, elastic, plastic, electrochemical, ferroelectric, ferromagnetic, origins or their combinations. When $f^*_{\phi=0} \neq f^*_{\phi=1}$, the final term in Eq. 1 breaks the symmetry of $f_b(\phi)$ (see Fig. 2) and with one of the phases occupying a lower minimum than the other, it defines the driving force for phase transformation in a PF model. The interpolant should have the properties of $h(\phi = 0) = 0$, $h(\phi = 1) = 1$ in addition to $h'(\phi = 0, 1) = 0$; the latter ensures that phase transformation happens only due to the migration of diffuse interfaces.

The evolution of the order parameter field follows the classical time-dependent Ginzburg–Landau dynamics and is determined by numerically integrating the Allen–Cahn equation[1],

$$\frac{\partial\phi}{\partial t} = -M\frac{\delta F}{\delta\phi} = -M\left(\frac{\partial f_b}{\partial\phi} - \kappa\nabla^2\phi\right), \tag{2}$$

which ensures that the evolution of $\phi(\boldsymbol{x}, t)$ field leads to a minimization of the free energy of the entire system. It must be noted that often the formulation of a PF model is stated in terms of the entropy density (s) instead of the free energy density (f) and the counterpart of Eq. 2 derived for that case leads to a maximization of the total entropy of the system[81]. The term $\delta F/\delta\phi$ in Eq. 2 indicates the variational derivative of the total free energy F with respect to the phase-field variable ϕ which on evaluation leads to the second equality in Eq. 2 with M denoting the interface mobility. Eq. 2 should be solved in unison with the evolution equations for the independent variables determining the free energy densities $f^*_{\phi=0,1}$, e.g., the solute and temperature fields need to be solved for simulating a phase transformation driven by differences in chemical free energy densities of phases. This particular variety of the PF model is classified as Model C by Halperin, Hohenberg[37] and its structure is replicated by most generic multiphase, multicomponent PF models.

It is important to note that the discussion in the previous paragraph is specific to models involving non-conserved order parameters derived from a top-down approach. The formulation will undergo changes when we consider models with conserved order parameters as the governing equation for its evolution will be based on a continuity equation, e.g., in the CH model the evolution of order parameters is given by[11],

$$\frac{\partial\phi}{\partial t} = -\nabla\cdot\mathbf{J} = \nabla\cdot\left(M\nabla\frac{\delta F}{\delta\phi}\right), \tag{3}$$

where, $\mathbf{J} = -M\nabla\dfrac{\delta F}{\delta\phi}$ is the solute mass flux related linearly to its thermodynamic driving force $\nabla\dfrac{\delta F}{\delta\phi}$ through solute mobility denoted by (M). The quantity $\dfrac{\delta F}{\delta\phi}$ denotes the solute diffusion

potential ($\widetilde{\mu}$). The Cahn–Hilliard model belongs to the class of Model B type PF formulations[37].

We are now in a position to consider generic multiphase, multicomponent PF models. All the three models discussed next are Model C type PF models and follow the same structure discussed in this section. It must be mentioned that the models as presented are valid only for substitutional solutes. Model extensions in literature to consider interstitial elements are referred to wherever applicable. With this background, we begin with a brief review of the Nestler, Garcke, Stinner model in the next section.

4 Nestler, Garcke, Stinner (NGS) model

One of the earliest PF models of multiphase, multicomponent systems is the one by Nestler, Garcke and Stinner[78, 97]. The model describes phase transformations involving N different phases through evolution of their respective order parameter fields represented vectorially as, $\boldsymbol{\phi} = \{\phi^1(\boldsymbol{x},t), \phi^2(\boldsymbol{x},t), \ldots, \phi^N(\boldsymbol{x},t)\}$. The values $\phi^\alpha = 1$ and $\phi^\alpha = 0$ indicate the presence and absence of the α phase at a particular point in the microstructure. The diffuse interface marking the transition from phase α to any other phase corresponds to the range of values, $0 < \phi^\alpha < 1$. The values of the order parameters $\boldsymbol{\phi}$ also represent the respective phase fractions at a particular point in the microstructure obeying the constraint, $\sum_{\alpha=1}^{N} \phi^\alpha = 1$. The spatio-temporal evolution of order parameter fields intend to maximize the entropy functional (S) stated as an integral over the entire system domain (Ω)[78],

$$S(e,\boldsymbol{c},\boldsymbol{\phi}) = \int_\Omega \Big[s(e,\boldsymbol{c},\boldsymbol{\phi}) - \left(\epsilon a(\boldsymbol{\phi},\nabla\boldsymbol{\phi}) + \frac{1}{\epsilon} w(\phi)\right)\Big] d\Omega. \tag{4}$$

In the above equation (Eq. 4), s is the entropy density term and is a function of the overall alloy composition (in terms of mole fractions) at every point in the microstructure denoted vectorially in the form, $\boldsymbol{c} = \{c_1, c_2, \ldots, c_k\}$ for a $(k+1)$ component alloy, where the solvent mole fraction is given by $c_0 = 1 - \sum_{i=1}^{k} c_i$. Additionally, s is also a function of the internal energy density (e) and the order parameter fields ($\boldsymbol{\phi}$). The last two terms in the integrand in Eq. 4 represent the entropy density terms leading to the formation of a diffuse interface between the phases. The width of the diffuse interface is a function of the parameter ϵ. The gradient entropy density term is written as[78],

$$a(\boldsymbol{\phi},\nabla\boldsymbol{\phi}) = \sum_{\alpha=1}^{N}\sum_{\beta<\alpha} \sigma_{\alpha\beta}\left[a_{\alpha\beta}(\mathbf{q}_{\alpha\beta})\right]^2 |\mathbf{q}_{\alpha\beta}|^2, \tag{5}$$

where, $\mathbf{q}_{\alpha\beta} = \phi^\alpha \nabla\phi^\beta - \phi^\beta \nabla\phi^\alpha$, represents the interfacial gradient vector which is oriented normal to the $\alpha-\beta$ interface, $\sigma_{\alpha\beta}$ is the entropy density associated with the $\alpha-\beta$ interface. The anisotropy of the interface is determined by the function $a_{\alpha\beta}(q_{\alpha\beta})$ which is set to unity for isotropic interfaces. The entropy density term $w(\boldsymbol{\phi})$ can be expressed as a multi-obstacle potential given by [78],

$$w(\boldsymbol{\phi}) = \frac{16}{\pi^2}\sum_{\alpha=1}^{N}\sum_{\beta<\alpha} \sigma_{\alpha\beta}\phi^\alpha\phi^\beta, \tag{6}$$

for microstructural states lying inside the Gibbs simplex, i.e., for $0 \le \phi^\alpha \le 1, \forall\alpha \in \{1,2,\ldots,N\}$, $\sum_{\alpha=1}^{N}\phi^\alpha = 1$, while, $w(\boldsymbol{\phi}) \to \infty$ for states lying outside, $\sum_{\alpha=1}^{N}\phi^\alpha > 1$. The other option is to use a multi-well potential[78],

$$w(\boldsymbol{\phi}) = 9\sum_{\alpha=1}^{N}\sum_{\beta<\alpha} \sigma_{\alpha\beta}(\phi^\alpha)^2(\phi^\beta)^2. \tag{7}$$

The resultant topology of the $w(\boldsymbol{\phi})$ hypersurface due to Eqs. 6 and 7 is such that an appearance of a spurious third phase across the $\alpha-\beta$ interface leads to a lower interfacial energy. Higher order polynomial terms in the order parameters can be added to these potentials in order to raise the energy of such spurious multiphase combinations leading to eventual suppression of their formation[78]. The evolution equations of the order parameter fields ensure a monotonic increase in the total entropy (S) of the system and are stated as[78, 97],

$$\begin{aligned}\tau\epsilon\frac{\partial\phi^\alpha}{\partial t} &= \frac{\delta S}{\delta\phi^\alpha} - \Lambda,\\ \tau\epsilon\frac{\partial\phi^\alpha}{\partial t} &= \epsilon\left(\nabla\cdot\frac{\partial a(\boldsymbol{\phi},\nabla\boldsymbol{\phi})}{\partial\nabla\phi^\alpha} - \frac{\partial a}{\partial\phi^\alpha}\right)\\ &\quad - \frac{1}{\epsilon}\frac{\partial w}{\partial\phi^\alpha} + \frac{\partial s}{\partial\phi^\alpha} - \Lambda,\ \forall\alpha\in\{1,2,\ldots,N\},\end{aligned} \tag{8}$$

where, Λ is a Lagrange parameter introduced so that the order parameter fields ($\boldsymbol{\phi}$) conform to the constraint $\sum_{\alpha=1}^{N}\phi^\alpha = 1$ during the course of their evolution and is set equal to the average of the RHS of Eq. 8 written for all the phases $\alpha \in \{1,2,\ldots,N\}$. The inverse of the parameter τ determines the mobility of the diffuse interface.

The knowledge of the functions $a(\boldsymbol{\phi}, \nabla\phi)$ and $w(\boldsymbol{\phi})$ allows us to determine the first (in parenthesis) and second terms in the RHS of Eq. 8. We can evaluate the term $(\partial s/\partial\phi^{\alpha})$ from a knowledge of the bulk entropy density function $s(e, \boldsymbol{c}, \boldsymbol{\phi})$ by relating it to the Helmholtz free energy density[97],

$$f(\boldsymbol{c}, \boldsymbol{\phi}) = e - Ts, \tag{9}$$

where, T is the temperature, and it can be rearranged to write,

$$s(\boldsymbol{c}, \boldsymbol{\phi}) = \frac{1}{T}\big(e - f(\boldsymbol{c}, \boldsymbol{\phi})\big), \tag{10}$$

and the derivative w.r.t ϕ can be evaluated as,

$$\frac{\partial s}{\partial \phi} = -\frac{1}{T}\frac{\partial f}{\partial \phi}. \tag{11}$$

Thus, the final form of the evolution equation for the order parameter fields (Eq. 8) is expressed as,

$$\begin{aligned}\tau\epsilon\frac{\partial\phi^{\alpha}}{\partial t} &= \epsilon\left(\nabla\cdot\frac{\partial a(\boldsymbol{\phi}, \nabla\boldsymbol{\phi})}{\partial\nabla\phi^{\alpha}} - \frac{\partial a}{\partial\phi^{\alpha}}\right)\\ &\quad - \frac{1}{\epsilon}\frac{\partial w}{\partial\phi^{\alpha}} - \frac{1}{T}\frac{\partial f}{\partial\phi^{\alpha}} - \Lambda,\\ &\quad \forall\alpha \in \{1, 2, \ldots, N\}.\end{aligned} \tag{12}$$

The derivative $\partial f/\partial\phi^{\alpha}$ in the above equation is evaluated from an expression of the free energy of the system written as an interpolation of the individual phase free energies[78],

$$\begin{aligned}f &= \sum_{\alpha=1}^{N} h^{\alpha}(\boldsymbol{\phi}) f^{\alpha} = \sum_{\alpha=1}^{N}\sum_{i=1}^{k}\left(c_i L_i^{\alpha}\frac{T - T_i^{\alpha}}{T_i^{\alpha}}h^{\alpha}(\boldsymbol{\phi})\right)\\ &\quad + \frac{RT}{V_m}\sum_{i=1}^{k} c_i \ln c_i - C_v \ln\left(\frac{T}{T_M}\right),\end{aligned} \tag{13}$$

where, individual phases are treated as regular solutions,

$$\begin{aligned}f^{\alpha}(\boldsymbol{c}, T, T_i^{\alpha}, L_i^{\alpha}) &= \sum_{i=1}^{k}\left[\left(c_i L_i^{\alpha}\frac{T - T_i^{\alpha}}{T_i^{\alpha}}\right) + \frac{RT}{V_m}c_i \ln c_i\right]\\ &\quad - C_v \ln\left(\frac{T}{T_M}\right),\end{aligned} \tag{14}$$

with the interpolant function chosen such that $\sum_{\alpha=1}^{N} h^{\alpha}(\boldsymbol{\phi}) = 1$ along with the properties of $h^{\alpha}(\phi^{\alpha} = 1) = 1$, $h^{\alpha}(\phi^{\alpha} = 0) = 0$ and $\partial h^{\alpha}/\partial\phi^{\alpha} = 0$ for $\phi^{\alpha} = 1, 0$. An example of such an interpolant is presented later in Eq. 29. The first term in Eq. 14 represents the interpolation of the free energies of the pure components in a particular phase α. The second term is the free energy of mixing and the third term represents the temperature (T) dependence of the phase free energy with C_V being the specific heat at constant volume and R being the gas constant. The molar volume represented by V_m is assumed to be a constant independent of composition and temperature in order to neglect the complicating influence of hydrodynamic flow on the solidification process. The above expression assumes that component i melts at the temperature T_i^{α} with a latent heat per unit volume indicated by L_i^{α}; the phase index N represents the liquid phase which acts as the thermodynamic reference with $L_i^{N} = 0$. It is evident from Eq. 14 that every participating phase in the multiphase mixture at a point in the microstructure shares the same composition c_i as that of the overall alloy composition. Hence Eq. 13 behaves as the multicomponent counterpart of the PF model for solidification proposed by Wheeler et al.[103] for binary alloys. Consequently, in the NGS model, the phases have unequal diffusion potentials across the regions of their coexistence which in any PF model corresponds to the diffuse interfaces and their intersections. This apparent lack of local equilibrium between the phases leads to an extra chemical energy contribution to the interfacial energy which scales with the size of the diffuse interface restricting the scalability of the interface width required to meet computational demands. This particular issue has been identified[56] and redressed in later PF models of alloys[18, 28, 57, 82]. The PF evolution equations (Eq. 12) are solved in unison with the energy and mass balance equations to determine the temperature (T) and composition $(\boldsymbol{c})$ fields, respectively. These conservation equations are derived variationally[97] in a manner analogous to that of Eq. 8 and can be stated as,

$$\frac{\partial e}{\partial t} = -\nabla\cdot\left[M_{00}\nabla\frac{1}{T} + \sum_{j=1}^{k} M_{0j}\nabla\left(\frac{-\mu_j}{T}\right)\right], \tag{15}$$

$$\frac{\partial c_i}{\partial t} = -\nabla\cdot\left[M_{i0}\nabla\frac{1}{T} + \sum_{j=1}^{k} M_{ij}\nabla\left(\frac{-\mu_j}{T}\right)\right], \tag{16}$$

where, the symmetric and positive semi-definite mobility matrix $[M]$ linearly relates the thermodynamic driving forces of $\nabla\frac{\delta S}{\delta e} = 1/T$ and $\nabla\frac{\delta S}{\delta c_i} = -\mu_i/T$ to heat and mass fluxes. The

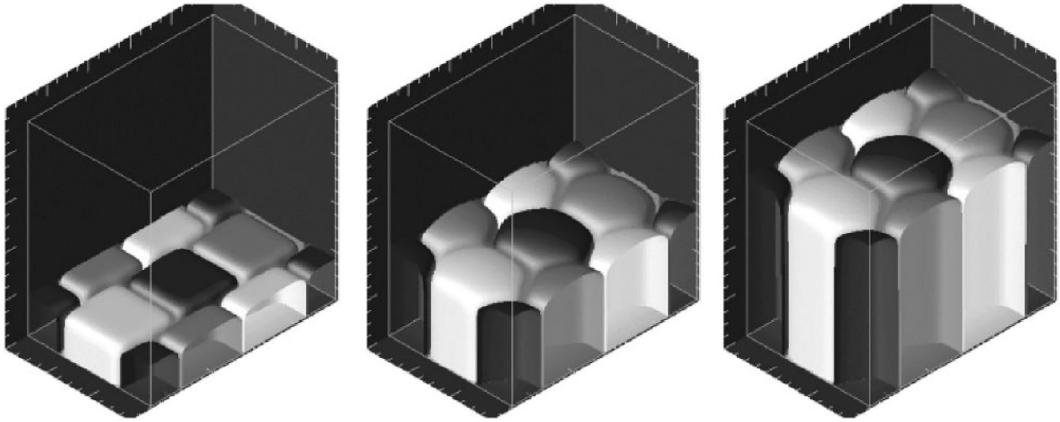

Figure 3: A PF simulation of ternary rod eutectics. Reprinted with permission from[78] DOI: https://doi.org/10.1103/PhysRevE.71.041609 Copyright (2005) by the American Physical Society.

diagonal components in the mobility matrix $[M]$, relate the energy and mass fluxes to their corresponding driving forces, while the off-diagonal terms give rise to cross-dependencies. Eqs. 12, 15and 16 are numerically integrated in a staggered manner to simulate phase transformations. An increased computational efficiency can be achieved by using the obstacle potential (Eq. 6) as then the PF evolution equations (Eq. 12) only need to be integrated over the diffuse interfaces.

4.1 Studies Using the NGS Model

The NGS model has been extensively used to simulate phase transformations in binary alloys[19, 32, 102] while studies in multicomponent systems are comparatively smaller in number. Interesting applications of the NGS model in the domain of multicomponent systems include simulations of transition from dendritic to globular morphologies during solidification of Ni-Cr-Cu alloys[25, 26] and dendritic structures in metallic glass matrix composite[43]. Noteworthy studies of multiphase solidification in multicomponent alloys using the NGS model include simulations of two-phase eutectic growth in the presence of a ternary impurity[78] and solidification of three-phase lamellar eutectic under stable[20, 78] and oscillatory growth modes[20]. A simulation of steady-state ternary eutectic growth reproduced from[78] is presented in Fig. 3.

5 Eiken, Böttger, Steinbach (EBS) Model

Eiken, Böttger, and Steinbach[28] proposed a PF model (henceforth called the 'EBS' model) of multiphase transformation in a multicomponent alloy where every phase participating in a multiphase equilibrium possesses a distinct composition related to each other by the condition of local equilibrium, hence eliminating the chemical energy excess associated with the diffuse interfaces in the NGS model[78]. The condition of local equilibrium in addition to other modeling details will be briefly reviewed in the following paragraphs.

A set of order-parameter fields $\boldsymbol{\phi} = \{\phi^1(\boldsymbol{x}, t), \ldots, \phi^N(\boldsymbol{x}, t)\}$ again describe an N-phase system in the EBS model which simultaneously indicate the local phase fractions obeying the constraint $\sum_{\alpha=1}^{\nu} \phi^\alpha = 1$ at every point in the microstructure. An additional parameter ν, where $\nu \leq N$, is introduced indicating the number of phases coexistent at a particular point in the microstructure. For a multicomponent alloy with $(k+1)$ components, the phase composition is described by k independent solute mole fractions which can be succinctly represented using a vectorial notation, e.g., for phase α, $\boldsymbol{c}^\alpha = \{c_1^\alpha, c_2^\alpha, \ldots, c_k^\alpha\}$, while the solvent concentration is given by $c_0^\alpha = 1 - \sum_{i=1}^{k} c_i^\alpha$. The order parameter fields and the phase compositions define the free energy functional of the entire system (F) as,

$$F = \int_\Omega \left[f_{\text{int}}(\boldsymbol{\phi}, (\nabla \boldsymbol{\phi})) + f_{\text{chem}}(\boldsymbol{\phi}, \boldsymbol{c}^1, \ldots, \boldsymbol{c}^N) \right] d\Omega, \tag{17}$$

where f_{int} represents the terms which lead to the creation of a stable diffuse interface, and f_{chem} is the chemical free energy density of the alloy, which are integrated over the system domain Ω. The energy densities are expressed as[28],

$$f_{\text{int}} = \sum_{\alpha=1}^{\nu} \sum_{\beta=1,\neq\alpha}^{\nu} \frac{4\sigma_{\alpha\beta}}{\eta} \left[-\frac{\eta^2}{\pi^2} \left(\nabla\phi_\alpha \cdot \nabla\phi_\beta \right) + \phi_\alpha \phi_\beta \right], \tag{18}$$

$$f_{\text{chem}} = \left[\sum_{\alpha=1}^{\nu} f^\alpha(\boldsymbol{c}^\alpha) \right] + \tilde{\boldsymbol{\mu}} \left(\boldsymbol{c} - \sum_{\alpha=1}^{\nu} \phi^\alpha \boldsymbol{c}^\alpha \right). \tag{19}$$

Two key parameters in Eq. 18 are that of the anisotropic interfacial energy ($\sigma_{\alpha\beta}$) of the $\alpha-\beta$ interface and the width of the diffuse interface (η) where the latter is treated as a constant regardless of the phases it separates. The expression of the total chemical free energy density f_{chem} (Eq. 19) consists of two terms; the first is an interpolation of the chemical free energy densities of the individual phases denoted by $f^\alpha(\boldsymbol{c}^\alpha)$, while the second penalizes any deviation in the overall composition of a multi-phase mixture $\boldsymbol{c} = \{c_1, c_2, \ldots, c_k\}$ from a weighted sum of the individual phase concentrations, through a Lagrange multiplier of the alloy diffusion potentials $\tilde{\boldsymbol{\mu}} = \{\widetilde{\mu_1}, \widetilde{\mu_2}, \ldots, \widetilde{\mu_k}\}$. The PF evolution equations are obtained by solving for the motion of all possible interfaces in the system and superimposing them[92],

$$\begin{aligned} \dot{\phi^\alpha} &= \frac{\pi^2}{8\eta} \sum_{\beta=1}^{\nu} M_{\alpha\beta} \left(\frac{\delta F}{\delta \phi^\alpha} - \frac{\delta F}{\delta \phi^\beta} \right), \\ \dot{\phi^\alpha} &= \sum_{\beta=1}^{\nu} \frac{M_{\alpha\beta}}{\nu} \left[\sum_{\gamma=1}^{\nu} \left(\sigma_{\beta\gamma} - \sigma_{\alpha\gamma} \right) I_\gamma \right. \\ &\quad \left. + \frac{\pi^2}{8\eta} \sqrt{\phi^\alpha \phi^\beta} \Delta G^{\alpha\beta} \right], \end{aligned} \tag{20}$$

$\forall \alpha \in \{1, \ldots, N\}$, where, $I_\gamma = \nabla^2 \phi^\gamma + \frac{\pi^2}{\eta^2} \phi^\gamma$ and the factor $\sqrt{\phi^\alpha \phi^\beta}$ is introduced in an ad-hoc manner to concentrate the driving forces at the interface. The mobility of the $\alpha-\beta$ interface indicated by $M_{\alpha\beta}$ can be an anisotropic function and along with the interfacial energy term $\sigma_{\alpha\beta}$ they are set to zero for identical values of the phase indices. $\Delta G^{\alpha\beta}$ is the driving force for $\alpha-\beta$ phase transformation expressed as[28],

$$\begin{aligned} \Delta G^{\alpha\beta} &= -\left(\frac{\partial}{\partial \phi^\alpha} - \frac{\partial}{\partial \phi^\beta} \right) f_{\text{chem}}, \\ &= \frac{1}{V_m} \left[\left(G^\beta(\boldsymbol{c}^\beta) - \tilde{\boldsymbol{\mu}} \boldsymbol{c}^\beta \right) - \left(G^\alpha(\boldsymbol{c}^\alpha) - \tilde{\boldsymbol{\mu}} \boldsymbol{c}^\alpha \right) \right], \end{aligned} \tag{21}$$

where $G^\alpha = V^m f^\alpha$ are the molar free energies of the phases with V_m representing the constant molar volume. Clearly, when G represents the molar Gibbs free energy of a phase, $\Delta G^{\alpha\beta}$ is the difference in the solvent chemical potentials of the phases α and β which only goes to zero when the two phases are in total equilibrium with each other and not just locally (see Fig. 5). The condition of local equilibrium on the other hand implies that solute exchange between phases present at a particular point in the microstructure happens instantaneously compared to the phenomena of interface migration and long range solute diffusion inside individual phases. As a result, the individual component diffusion potentials of every phase ($\widetilde{\boldsymbol{\mu}^\alpha}$) present at a point are equal to each other which in turn fixes the individual phase compositions in a multiphase equilibrium. The equality of only the component diffusion potentials but not of the corresponding chemical potentials or the more general quantity of grand potential densities of the phases is termed as the "quasiequilibrium" condition by Eiken et al.[28] and can be mathematically stated for a ν phase mixture as[9,28],

$$\begin{aligned} &\widetilde{\boldsymbol{\mu}^1} = \widetilde{\boldsymbol{\mu}^2} = \cdots = \widetilde{\boldsymbol{\mu}^\nu}, \\ &\implies \frac{\partial G^1}{\partial \boldsymbol{c}^1} = \frac{\partial G^2}{\partial \boldsymbol{c}^2} = \cdots = \frac{\partial G^\nu}{\partial \boldsymbol{c}^\nu}, \end{aligned} \tag{22}$$

with the multiphase mixture composition given by[28],

$$\boldsymbol{c} = \sum_{\alpha=1}^{\nu} \phi^\alpha \boldsymbol{c}^\alpha. \tag{23}$$

Considering $(\nu-1)k$ equations of local equilibrium between individual phases from Eq. 22 and k equations from Eq. 23 a system of νk equations at every point in the microstructure containing a mixture of multiple phases can be obtained, from which an identical number of unknowns of phase compositions can be determined. The evolution of the overall alloy composition ($\boldsymbol{c}$) is obtained by solving the diffusion equation given as[28],

$$\dot{\boldsymbol{c}} = \nabla \sum_{\alpha=1}^{\nu} \phi^\alpha [D^\alpha] \{\nabla \boldsymbol{c}^\alpha\}, \tag{24}$$

where $[D^\alpha]$ represents the $k \times k$ solute interdiffusivity matrix in the α phase, while $\nabla \boldsymbol{c}^\alpha$ represents the composition gradients in the α phase. The crux of the EBS model is described by Eqs. 20, 22, 23 and 24 and staggered solutions of these equations lead to simulations of isothermal phase transformation in multi-component alloys. Non-isothermal transformations can be modeled by imposing a temperature field T as

in simulations of directional solidification or by coupling a thermal diffusion equation to the set of Eqs. 20, 22, 23 and 24. The prohibitively high computational cost associated with the iterative solution of the set of nonlinear equations given by Eq. 22 (and Eq. 23) prompted the development of linear extrapolation schemes[28] to approximate phase compositions under quasiequilibrium. Thus, a computationally efficient approach solves Eqs. 22 sparingly, while for the majority of the timesteps estimates phase compositions through appropriate extrapolation schemes. Such a hybrid scheme leads to a computationally efficient imposition of quasiequilibrium while maintaining the sanctity of the thermodynamic description of the alloy system.

The EBS model requires thermodynamic inputs of the molar Gibbs free energies of the phases as functions of the compositions and temperature ($G^{\alpha}(\boldsymbol{c}^{\alpha}, T)$) and kinetic inputs of solute interdiffusivities (D_{ij}^{α}) which can be obtained from CALPHAD (CALculation of PHAse Diagrams)[70, 87] based databases of thermodynamic and kinetic[3] data. The software MICRESS®(MICRostructure Evolution Simulation Software)[72], which solves the EBS model in conjunction with ThermoCalc®[4] for thermodynamic and kinetic inputs, is a leading exponent of the concept of runtime information exchange between a PF model and a CALPHAD based database. This concludes the brief review of the EBS model, and we will now summarize a few important PF studies performed using the EBS model in the following subsection.

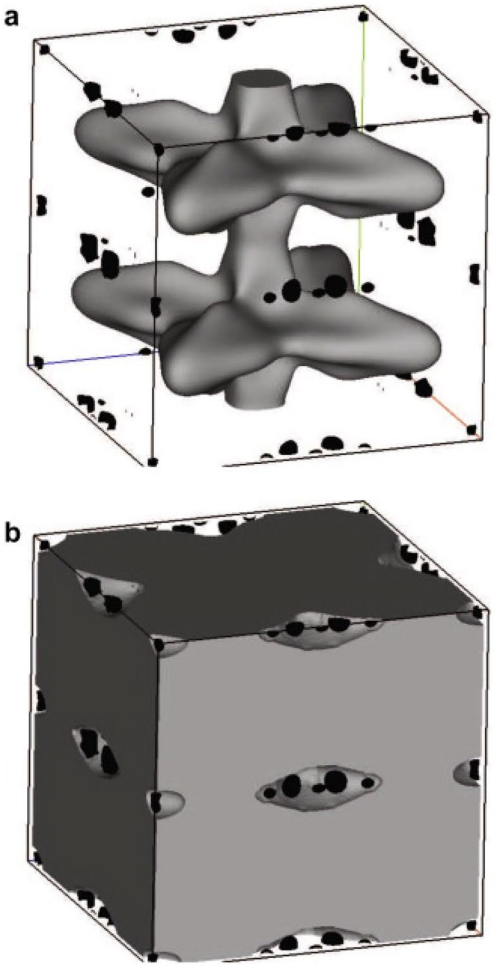

Figure 4: Simulation of interdendritic γ' phase formation in Ni base superalloys. Reprinted from[101], Copyright (2009), with permission from Elsevier.

5.1 Studies using/extending the EBS model

There are several interesting simulations of microstructure formation in multicomponent alloys that have been performed using the EBS model. These include simulations of constrained and equiaxed dendritic growth during solidification of multicomponent alloy systems like Ni-base (Ni-Al-Cr-Ta-W) superalloys[101], Al-Mg-Zn[8, 93], Al-Si-Cu-Mg-Ni[8]. Studies have also simulated the solidification sequence to a considerable extent like the formation of interdendritic γ' phases in Ni-Al-Cr-Ta-W superalloys[101] as reproduced in Fig. 4 and the sequence and morphology of different phases in Al-Si-P and Al-Si-P-Sr alloys[29].

A few studies also led to the further development of the EBS model. A key work in this regard is the formulation of an anti-trapping current to negate the anomalous solute trapping at migrating diffuse interfaces[13]. Although the linearized extrapolation schemes to approximate quasiequilibrium conditions in the EBS model offer a significant computational advantage over solving a system of nonlinear equations (Eq. 22), they themselves involve inversions of $k \times k$ matrices where k indicates the number of solutes. So, such approximation schemes are bound to become computationally expensive as the number of solutes (k) increases. This has prompted the introduction of several secondary assumptions to speed up the calculations[28] with a possible compromise in numerical accuracy. Bottger et al.[9] implemented an analytically simplified version of the extrapolation scheme in its most general form for a ternary alloy and found simulations to retain its accuracy even with fewer calls to direct imposition of quasiequilibrium

(Eqs. 22, Eq. 23). A Taylor Series based extrapolation scheme for a generic multicomponent alloy providing improved accuracy is also proposed recently[104] A recent work extends the EBS formulation to include the effects of elastic strain energy gradients as driving forces for phase transformation and solute diffusion[10]. In addition to the aforementioned studies, the EBS model has been modified to allow simulations of materials phenomena which involve deviations from equilibrium at the diffuse interface. Such developments are taken up in the next subsection.

5.2 Extending EBS Model to Include Interface Dissipation

The EBS model assumes that the phases coexisting at a particular point in the microstructure are in local equilibrium with each other given by the equality of component diffusion potentials in the participating phases (Eq. 22). Local equilibrium at the interface is a consequence of much faster solute diffusion compared to the rate of interface migration. But when the interface velocity (V) becomes of the same order as that of the rate of solute diffusion (D/η) across the interface, solute exchange across the moving interface is limited and may not lead to equilibrium compositions of the phases. Thus, it becomes critical to solve for the kinetics of solute diffusion explicitly to determine the exact extent of deviation from equilibrium at the interface. In summary, for interface velocities comparable to or greater than the rate of solute diffusion, phase compositions are no longer coupled to each other through the condition of local equilibrium and the component diffusion potentials of the coexisting phases are unequal to each other, i.e., $\widetilde{\boldsymbol{\mu}^{\alpha}} \neq \boldsymbol{\mu}^{\beta}$. Steinbach et al.[94] and Zhang, Steinbach[105] extended the EBS model to develop a PF model capable of handling such deviations from local equilibrium at the interfaces. According to these studies, a PF model of rapid transformation should consider individual phase compositions as independent entities with their own evolution equations. Furthermore, the process of solute exchange between coexistent phases should be modeled explicitly and associated with a finite time scale. Both these features are incorporated into the framework of the EBS model to develop models with finite interface dissipation specifically for two phase equilibrium in binary alloys[94] and for multiple phases in multicomponent alloys[105]. In the latter, the chemical free energy density is given as,

$$f_{\text{chem}} = \left[\sum_{\alpha=1}^{\nu} \phi^{\alpha} f^{\alpha}(\boldsymbol{c}^{\alpha})\right] + \boldsymbol{\lambda}\left(\boldsymbol{c} - \sum_{\alpha=1}^{\nu} \phi^{\alpha}\boldsymbol{c}^{\alpha}\right), \tag{25}$$

where, $\boldsymbol{\lambda} = \{\lambda_1, \lambda_2, \cdots, \lambda_k\}$ indicates the vector of Lagrange multipliers which in contrast to the EBS model[28] are in general not equal to the diffusion potentials $\tilde{\boldsymbol{\mu}}$ (see Eq. 19). The parameters $\boldsymbol{\lambda}$ are determined from the overall compositional invariance of the multiphase mixture at a particular point in the microstructure considering the exchange of solutes between the participating phases and the solute rejection due to phase transformation. The evolution of individual phase compositions are given by[105],

$$\phi^{\alpha}\dot{\boldsymbol{c}^{\alpha}} = \nabla \cdot \left([D^{\alpha}]\{\nabla \boldsymbol{c}^{\alpha}\}\right) + \sum_{\beta=1}^{\nu} \boldsymbol{P}\phi^{\alpha}\phi^{\beta}\left(\widetilde{\boldsymbol{\mu}^{\beta}} - \widetilde{\boldsymbol{\mu}^{\alpha}}\right) - \sum_{\beta=1}^{\nu} \phi^{\alpha}\dot{\phi^{\beta}}\left(\boldsymbol{c}^{\beta} - \boldsymbol{c}^{\alpha}\right). \tag{26}$$

The first term on the RHS indicates solute redistribution due to diffusion within a particular phase α. The second term considers the possibility that the phase diffusion potentials are dissimilar from each other, i.e., $\mu_i^{\beta} \neq \widetilde{\mu_i^{\alpha}}$, driving solute exchange between the coexistent phases whose rates are determined by the interface permeabilities $\boldsymbol{P} = \{P_1, P_2, \ldots, P_k\}$ of the individual solutes. The interface permeabilities are determined from an atomistic-level consideration of the phenomenon of solute diffusion between the phases[94]. The third term in Eq. 26 represents the influence of the rejected solute due to phase transformation on the composition of phase α. The evolution equations for the phase-fields ϕ^{α} are derived following the same procedure as in the EBS model[28] and are rearranged to identify interface mobilities as functions of the kinetic parameters $\boldsymbol{P}$. At the limit of $\boldsymbol{P} \to \infty$, the phases are in local equilibrium across the interface and the original EBS model is recovered. Conversely, in the limit of $\boldsymbol{P} \to 0$, there is complete solute trapping and leads to frozen order parameter fields[94, 105].

An alternate set of evolution equations for the phase compositions are derived by conserving solute concentrations for every two phase equilibrium in the multiphase mixture[105] in the spirit of the multiphase-field (MPF) model[92]. The new set of composition evolution equations allow the additional flexibility of choosing a distinct set of kinetic parameters $\boldsymbol{P}^{\alpha\beta}$ for every interface which separates a particular combination of phases (α and β) in contrast to the constant $\boldsymbol{P}$ discussed

in the context of Eq. 26. The model considering finite interface dissipation for multicomponent alloys[105] is also coupled to CALPHAD based sublattice models for thermodynamic input to simulate the growth of stoichiometric phases[106]. This completes our review of the EBS model and its extensions. In the next section, we will take up the Grand-Potential model.

6 The Grand-Potential (GP) Model

The latest entrant in the domain of multiphase field models for multicomponent alloys is the Grand-Potential model (henceforth called the GP model) developed independently by Plapp[82] and Choudhury, Nestler[18], and as its name suggests it is based on a grand potential density rather than free energy[28] or entropy densities[78]. The advancement made by the GP model can be appreciated in the context of the EBS and the NGS models. Both the NGS[78] and the EBS[28] models involve respectively the overall alloy composition and the individual phase compositions as independent model variables in addition to the order parameter fields. The NGS model assumes that all coexisting phases at a particular point in the microstructure have the same composition and hence the phases participating in a multiphase mixture cannot assume disparate compositions corresponding to common diffusion potentials. As a result, the phases coexist with non-equilibrium compositions and contribute spurious chemical free energy to the energy of the diffuse interfacial regions in a PF microstructure, thus lowering the quantitative accuracy of PF simulations with artificially large interface widths. The EBS model corrects this anomaly by introducing individual phase solute concentrations as independent variables instead of the overall alloy composition, which in a multiphase mixture are related to each other through the condition of local equilibrium, i.e., through equality of phase diffusion potentials. As discussed in Sect. 5, the only difficulty with this approach is the high computational cost associated with the imposition of local equilibrium requiring iterative solution of a system of nonlinear equations (Eq. 22). The Grand-potential model[18, 82] (or the GP model) obviates this necessity of explicitly imposing the condition of local equilibrium by replacing the phase compositions with their corresponding conjugate intensive variables of diffusion potentials ($\widetilde{\boldsymbol{\mu}}$) as independent variables. It is important to note that the diffusion potentials

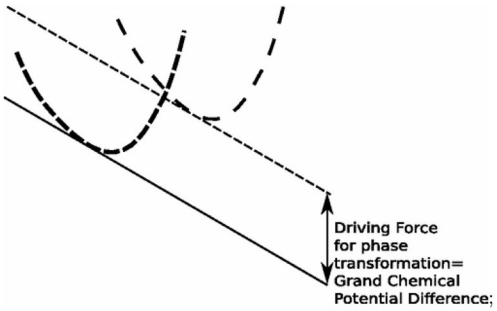

Figure 5: Schematic of a free energy versus composition diagram highlighting the driving force for phase transformation as difference in grand potential densities. Reprinted figure with permission from[18] DOI:https://doi.org/10.1103/PhysRevE.85.021602 Copyright (2012) by the American Physical Society.

are equal to each other in any N-phase equilibrium, i.e., $\widetilde{\boldsymbol{\mu}}^1 = \widetilde{\boldsymbol{\mu}}^2 = \cdots = \widetilde{\boldsymbol{\mu}}^N$. In other words, the composition vectors of $\boldsymbol{c}^1, \boldsymbol{c}^2, \ldots, \boldsymbol{c}^N$ for each of the N phases in the microstructure are now determined as functions of a single vector of diffusion potentials $\widetilde{\boldsymbol{\mu}}$ ($= \widetilde{\boldsymbol{\mu}}^1 = \widetilde{\boldsymbol{\mu}}^2 = \cdots = \widetilde{\boldsymbol{\mu}}^N$ for an N-phase equilibrium), i.e., $\boldsymbol{c}^\alpha \equiv \boldsymbol{c}^\alpha(\widetilde{\boldsymbol{\mu}}), \forall \alpha \in \{1, 2, \ldots, N\}$. It is important to note that phase-specific thermodynamic information is usually available in the form of functions $G(\boldsymbol{c})$, from which the functional relationship $\widetilde{\boldsymbol{\mu}} = \partial G / \partial \boldsymbol{c} \equiv \widetilde{\boldsymbol{\mu}}(\boldsymbol{c})$, follows naturally. As such a relationship has to be inverted to get the required function $\boldsymbol{c} \equiv \boldsymbol{c}(\widetilde{\boldsymbol{\mu}})$, it becomes necessary for the function $G(\boldsymbol{c})$ to be convex (see Fig. 5 for an example) to ensure a unique mapping between $\widetilde{\boldsymbol{\mu}}$ and $\boldsymbol{c}$. As the driving forces for solute diffusion are determined by gradients in diffusion potentials, the choice of diffusion potentials $\widetilde{\boldsymbol{\mu}}$ as independent variables is conceptually equivalent to the choice of temperature (T) as the independent variable for determining energy redistribution in a PF model of non-isothermal transformation. Thus, unlike the EBS model, the condition of local equilibrium is implicit in the formulation of the GP model and its imposition does not require any additional computational effort. With this understanding of the key advancement made by the GP model, let us briefly review the model details in the following paragraph.

Our review of the GP model largely follows the work of Choudhury, Nestler[18] beginning with an expression of the Grand potential functional (Ω) of the system written as,

$$\Omega = \int_V \Big[\Psi(T,\mu,\phi) + \left(\epsilon a(\boldsymbol{\phi},\nabla\boldsymbol{\phi}) + \frac{1}{\epsilon}w(\boldsymbol{\phi})\right)\Big] \mathrm{d}V, \tag{27}$$

where, Ψ is the interpolated phase grand potential densities (Ψ^α),

$$\Psi = \sum_{\alpha=1}^{N} h^\alpha(\boldsymbol{\phi})\Psi^\alpha, \tag{28}$$

where, the interpolant functions are given by[17],

$$h^\alpha(\boldsymbol{\phi}) = (\phi^\alpha)^2(3-2\phi^\alpha) + 2\phi^\alpha \sum_{\beta=1,\beta\neq\alpha}^{N} \sum_{\gamma=1,\gamma\neq\alpha}^{N} \phi^\beta\phi^\gamma, \tag{29}$$

and the phase grand potential density (Ψ^α) is defined by a Legendre transform of the phase Helmholtz free energies given by,

$$\Psi^\alpha(\tilde{\boldsymbol{\mu}}) = f^\alpha(\tilde{\boldsymbol{\mu}}) - \frac{1}{V_m}\tilde{\boldsymbol{\mu}}\cdot\boldsymbol{c}^\alpha(\tilde{\boldsymbol{\mu}}), \tag{30}$$

using a vectorial notation. The rest of the terms in Eq. 27 lead to the creation of the diffuse interface and are notationally identical to their counterparts defined in the context of the entropy functional in Eq. 4. The definitions of the terms $a(\boldsymbol{\phi},\nabla\boldsymbol{\phi})$ and $w(\boldsymbol{\phi})$ are also the same as given by Eqs. 5, 6 and 7, except that they indicate grand potential densities instead of entropy densities. The phase compositions can be determined from Eq. 30 as,

$$\boldsymbol{c}^\alpha = -V_m\frac{\partial\Psi^\alpha}{\partial\tilde{\boldsymbol{\mu}}}, \tag{31}$$

which, can be interpolated to get the overall alloy composition as,

$$\boldsymbol{c} = \sum_{\alpha=1}^{N} h^\alpha(\boldsymbol{\phi})\boldsymbol{c}^\alpha. \tag{32}$$

The PF evolution equation for the GP model minimizes the grand-potential functional[18] and can be written as,

$$\tau\epsilon\frac{\partial\phi^\alpha}{\partial t} = -\frac{\delta\Omega}{\delta\phi^\alpha} - \Lambda = \epsilon\left(\nabla\cdot\frac{\partial a(\boldsymbol{\phi},\nabla\boldsymbol{\phi})}{\partial\nabla\phi^\alpha} - \frac{\partial a}{\partial\phi^\alpha}\right) - \frac{\partial w}{\partial\phi^\alpha} - \frac{\partial\Psi(\tilde{\mu},T,\phi)}{\partial\phi^\alpha} - \Lambda,\ \forall\alpha\in\{1,2,\ldots,N\} \tag{33}$$

where the purpose of parameter Λ is the same as in Eq. 12. The term $\partial\Psi/\partial\phi^\alpha$ encapsulates the driving force for phase transformation and is determined from the deviation of diffusion potentials from their equilibrium values $\tilde{\boldsymbol{\mu}}$. Inspecting a two phase $\alpha-\beta$ system, the total grand-potential density is given by, $\Psi = \Psi^\alpha h^\alpha + \Psi^\beta(1-h^\alpha(\boldsymbol{\phi}))$ and the derivative evaluates to $\partial\Psi/\partial\phi^\alpha = (\Psi^\alpha - \Psi^\beta)(\partial h^\alpha(\boldsymbol{\phi})/\partial\phi^\alpha)$. The driving force of phase transformation is given by the difference in grand-potential densities of the phases ($\Psi^\alpha - \Psi^\beta$) and is illustrated using the schematic in Fig. 5. The derivative of the interpolant ($\partial h^\alpha(\boldsymbol{\phi})/\partial\phi^\alpha$) concentrates the driving force at the diffuse interfaces. In comparison to the difference in grand-potential densities driving phase transformation in the GP model, the EBS model describes the driving force as a difference between the solvent chemical potentials of the phases. The difference between these two definitions of driving forces is negligibly small when we consider a transformation between phases sharing similar molar volumes while there can be non-trivial differences when we model phase transformations involving large changes in molar volumes.

The evolution of $\tilde{\boldsymbol{\mu}}$ is obtained by solving the diffusion equation[17],

$$\frac{\partial\tilde{\mu}_i}{\partial t} = \left[\sum_{\alpha=1}^{N} h^\alpha(\boldsymbol{\phi})\frac{\partial c_i^\alpha(\tilde{\boldsymbol{\mu}},T)}{\partial\widetilde{\mu_k}}\right]^{-1}_{ik} \Big\{\nabla\cdot\left([M_{kj}(\boldsymbol{\phi})]\{\nabla\widetilde{\mu_j}\} - \mathbf{j_k^{at}}\right) - \sum_{\alpha=1}^{N} c_k^\alpha(\tilde{\boldsymbol{\mu}},T)\frac{\partial h^\alpha(\boldsymbol{\phi})}{\partial t} - \frac{\partial T}{\partial t}\sum_{\alpha=1}^{N}\left(\frac{\partial c_k^\alpha(\tilde{\boldsymbol{\mu}},T)}{\partial T}\right)_{\tilde{\boldsymbol{\mu}}} h^\alpha(\boldsymbol{\phi})\Big\}, \tag{34}$$

where, $\mathbf{j_{at}}$ is the solute antitrapping current introduced to negate anomalous solute trapping across the diffuse interface. The mobility matrix $M_{ij}(\boldsymbol{\phi})$ is given by an interpolation of the individual phase mobility matrices M_{ij}^α,

$$M_{ij}(\boldsymbol{\phi}) = \sum_{\alpha=1}^{N} g^\alpha(\boldsymbol{\phi})M_{ij}^\alpha. \tag{35}$$

where, the individual phase mobilities can be obtained from phase interdiffusivities as,

$$M_{ij}^\alpha = [D_{ik}^\alpha]\left[\frac{\partial c_k^\alpha(\tilde{\boldsymbol{\mu}},T)}{\partial\widetilde{\mu_j}}\right], \tag{36}$$

and a possible choice for the interpolants can be given by $g^\alpha(\boldsymbol{\phi}) = \phi^\alpha$. The derivatives $\partial h^\alpha(\boldsymbol{\phi})/\partial t$ in Eq. 34 can be evaluated from a knowledge of $\partial\boldsymbol{\phi}/\partial t$ obtained from Eq. 33 establishing a clear bi-directional coupling between the the $\boldsymbol{\mu}$ and $\boldsymbol{\phi}$

evolution equations. For non-isothermal simulations, the $T(\boldsymbol{x}, t)$ field in combination with the $\tilde{\boldsymbol{\mu}}$ field determines the grand potential density (Ψ) in Eq. 33. The T and $\tilde{\boldsymbol{\mu}}$ fields are coupled to each other through the term containing the time derivative of T field in Eq. 34.

6.1 Studies Using the GP Model

The GP model has been used extensively to simulate solidification in multicomponent alloys. These studies can be broadly classified into two categories: those reporting simulations of solidification of a single solid phase from the melt and those studying simultaneous solidification of multiple phases from the melt. An interesting series of studies in the former category investigates the influence of solute interdiffusivity matrices on the entire solidification sequence leading to dendritic growth[64, 65, 67]. The first study in the sequence investigated the dependence of equilibrium compositions of the phases and characteristic scaling constants of isothermal growth on solute interdiffusivities during the stable growth regime in ternary alloys[67]. The understanding derived from this study is extended to an investigation of the behaviour of an infinitesimally perturbed solidification front of a model quaternary alloy. The effect of alloy thermodynamics and kinetics in determining the dominant wavelength of perturbation is calculated analytically from a linear stability analysis and the predictions are found to be in good agreement with simulations using the GP model[64]. The instabilities of the solidification front amplify with time and lead to complete breakdown of the interface forming dendrites. Free dendritic growth in a ternary melt under isothermal conditions is studied using the GP model to identify the nature of dependence of the dendrite tip-radius (R_{tip}) on kinetic and thermodynamic parameters of model ternary alloys and the predictions are compared against theoretical analyses[65].

Moving on to multiphase solidification in multicomponent alloys where there are several interesting studies using the GP model. Applications of the GP model include investigations of the morphologies of three-phase eutectics as functions of the volume fractions of the solid phases and the solid-liquid interfacial energies in ternary alloys like Ag-Al-Cu[17, 21, 39]. Simulated microstructures of three-phase ternary eutectics are found to be increasingly sensitive to the simulation set-up as the simulation box-sizes are made smaller. This underlines the importance of large scale simulations to gain an accurate understanding of phase morphologies[95]. Simulations have identified the spiral-like arrangement of two different solid-phase lamellae embedded in a third solid phase during directional solidification of ternary Ag-Al-Cu eutectics to be a consequence of the tilted growth modes of eutectic solidification[40]. The functional dependence of tilted growth modes on the relative magnitudes of the solid-liquid, solid-solid interfacial energies, and solute diffusivities, have also been studied by simulations using the GP model[79]. The effect of dynamic variations of pulling velocities on the solidification microstructures for the Ag-Al-Cu ternary eutectic is also reported[41]. Similar studies have also been performed for the two-phase eutectic in the NiAl-34Cr system[52, 53] culminating in simulations of eutectic colonies by coupling a nucleation scheme to the GP model[54]. Quantitative simulations from the GP model have also been used as a benchmark to compare the predictions from a generalized Jackson-Hunt[45] theory of steady-state eutectic growth involving an arbitrary number of solid phases growing in a generic multi-component alloy[63]. Similar comparisons have also been reported by Steinmetz et al.[96].

Other than solidification, the GP model has also been used to study precipitate growth and coarsening in multicomponent alloys[6, 7, 76].

On the model development side, there are continuous ongoing attempts to add more features to the GP model. An important study in this respect expands the ambit of the GP model to consider both substituitional and interstitial solutes[2]. Another development specifically includes interfacial diffusion in the GP model[36].

Like in the EBS[28] model, the GP model can also be coupled to thermodynamic databases. The coefficients in a Taylor series expansion of the free energy as a function of composition can be determined from thermodynamic databases which can then be used in the GP model to simulate transformations in real materials[17]. This manner of coupling is applicable to deviations from equilibrium small enough to be accurately described by a truncated Taylor series up to the second order term. Recently, an alternate mechanism of coupling has been reported. Here, the convex functions $G^{\alpha}(\boldsymbol{c})$ from databases are converted into $\Psi^{\alpha}(\boldsymbol{\mu})$ numerically, which are then directly utilized in simulations[15].

7 Other Models of Phase Transformations in Multicomponent Alloys

In the previous sections, we have briefly discussed those PF models of multiphase, multicomponent transformation which are completely generic and

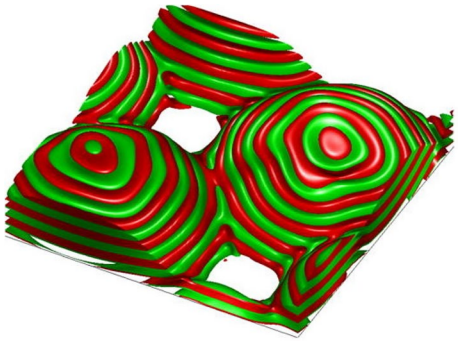

Figure 6: Simulated spiral dendrites. Figure reused[68] with permission from Elsevier.

can model arbitrary number of phases in an alloy with arbitrary number of solute components. Besides these models, the PF modeling literature contains many other interesting approaches to simulate phenomena in multi-component alloys, but which have not been posed in a generalized form. In this section, we briefly review such models.

Kim proposed a model of single-phase solidification in multicomponent alloys[55] as an extension of the binary alloy model presented earlier[57]. Another model of single phase solidification in multicomponent alloys is proposed by Emmerich et al.[60, 61]. Cha et al.[14] developed a model of single-phase solidification in multicomponent alloys considering both substitutional and interstitial solutes.

The Cahn–Hilliard (CH) model[11, 12] has also been used with success to simulate solid-state transformations in multicomponent alloys. The ability of the CH model to simulate systems with concavities in its free energy makes it an appropriate choice for simulating microstructures in phase separating systems in metallic[59] as well as polymeric/organic systems[33, 34, 46, 47]. Additionally, it has also been used to simulate precipitate coarsening in ternary alloys[7]. It is important to note that just like in the NGS model, there is a chemical energy contribution to the interfacial energy in the CH model which scales with the width of the interface. Thus, it is important to restrict the usage of CH models to experimentally verifiable interface widths.

A unique modeling approach coupling Allen–Cahn[1] and Cahn-Hilliard equations[11] is proposed to simulate colony formation during directional solidification of two-phase eutectics in the presence of a ternary impurity[83]. The overall motion of the solidification front is obtained from a solution of the Allen–Cahn equation while the Cahn–Hilliard equation controls the generation of new eutectic lamellae. This model has been extended by including the effects of kinetic[84, 86] and interfacial anisotropy[62, 68] to study the formation and scaling properties of spiral dendrites (see Fig. 6).

8 Conclusions and Outlook

We have traced the evolution of quantitative PF models which can tackle any number of components and phases. Coupling such a PF machinery with thermodynamic and kinetic databases results in predictive simulations of microstructure evolution in multicomponent alloys. Such simulations can be used to scan through the compositional and process variable spaces to decide the right combinations of alloy chemistry and processing routes for achieving the desired microstructure and properties. Although the true potential of phase-field modeling lies in providing guidelines for experimental design of alloys and their microstructures, such an approach is yet to be fully harnessed by the scientific community. Phase-field modeling is still primarily viewed as a tool to gain a deeper understanding of the process of genesis of microstructural features observed experimentally. However, an appreciation of its predictive power is bound to grow with time as the material science community confronts the impending challenge presented by the design of multicomponent alloys like "high entropy alloys (HEA)", and "complex concentrated alloys (CCA)" which offer exciting property profiles[35, 73, 85].

A purely experimental approach to design novel multicomponent alloys is a resource-intensive route. Using computational predictions to streamline experiments can drastically reduce costs and energy consumption and such a hybrid approach offers the most sustainable way to design novel alloys. In view of the versatility and quantitative accuracy of the PF models discussed in this review, it can be anticipated that simulations of microstructure evolution using such quantitative PF models will continue to accelerate the design and development of novel multicomponent alloys in the future.

Publisher's Note

Acknowledgements

Arka Lahiri gratefully acknowledges the financial support offered by FIG IIT Roorkee.

Declarations

Conflict of interest

On behalf of all authors, the corresponding author states that there is no conflict of interest.

Received: 28 July 2021 Accepted: 10 January 2022
Published: 20 March 2022

References

1. Allen SM, Cahn JW (1979) A microscopic theory for antiphase boundary motion and its application to antiphase domain coarsening. Acta Metall 27(6):1085–1095
2. Amos PK, Nestler B (2020) Grand-potential based phase-field model for systems with interstitial sites. Sci Rep 10(1):1–22
3. Andersson JO, Ågren J (1992) Models for numerical treatment of multicomponent diffusion in simple phases. J Appl Phys 72(4):1350–1355
4. Andersson JO, Helander T, Höglund L, Shi P, Sundman B (2002) Thermo-calc & dictra, computational tools for materials science. Calphad 26(2):273–312
5. Asta M, Beckermann C, Karma A, Kurz W, Napolitano R, Plapp M, Purdy G, Rappaz M, Trivedi R (2009) Solidification microstructures and solid-state parallels: recent developments, future directions. Acta Mater 57(4):941–971
6. Bhaskar M (2017) Effect of differential diffusivity on precipitate growth in ternary two-phase alloys: a phase field study. Philos Mag 97(19):1610–1627
7. Bhaskar M (2018) Quantitative phase field modelling of precipitate coarsening in ni-al-mo alloys. Comput Mater Sci 146:102–111
8. Böttger B, Eiken J, Steinbach I (2006) Phase field simulation of equiaxed solidification in technical alloys. Acta Mater 54(10):2697–2704
9. Böttger B, Eiken J, Apel M (2015) Multi-ternary extrapolation scheme for efficient coupling of thermodynamic data to a multi-phase-field model. Comput Mater Sci 108:283–292
10. Böttger B, Apel M, Budnitzki M, Eiken J, Laschet G, Zhou B (2020) Calphad coupled phase-field model with mechano-chemical contributions and its application to rafting of γ'in cmsx-4. Comput Mater Sci 184:109909
11. Cahn JW (1961) On spinodal decomposition. Acta Metall 9(9):795–801
12. Cahn JW, Hilliard JE (1958) Free energy of a nonuniform system. I. Interfacial free energy. J Chem Phys 28(2):258–267
13. Carré A, Böttger B, Apel M (2013) Implementation of an antitrapping current for a multicomponent multiphase-field ansatz. J Cryst Growth 380:5–13
14. Cha PR, Yeon DH, Yoon JK (2005) Phase-field model for multicomponent alloy solidification. J Cryst Growth 274(1–2):281–293
15. Chatterjee S, Moelans N (2021) A grand-potential based phase-field approach for simulating growth of intermetallic phases in multicomponent alloy systems. Acta Mater 206:116630
16. Chen LQ (2002) Phase-field models for microstructure evolution. Annu Rev Mater Res 32(1):113–140
17. Choudhury A (2015) Pattern-formation during self-organization in three-phase eutectic solidification. Trans Indian Inst Met 68(6):1137–1143
18. Choudhury A, Nestler B (2012) Grand-potential formulation for multicomponent phase transformations combined with thin-interface asymptotics of the double-obstacle potential. Phys Rev E 85(2):021602
19. Choudhury A, Nestler B, Telang A, Selzer M, Wendler F (2010) Growth morphologies in peritectic solidification of fe-c: a phase-field study. Acta Mater 58(10):3815–3823
20. Choudhury A, Plapp M, Nestler B (2011) Theoretical and numerical study of lamellar eutectic three-phase growth in ternary alloys. Phys Rev E 83(5):051608
21. Choudhury A, Yabansu YC, Kalidindi SR, Dennstedt A (2016) Quantification and classification of microstructures in ternary eutectic alloys using 2-point spatial correlations and principal component analyses. Acta Mater 110:131–141
22. Collins JB, Levine H (1985) Diffuse interface model of diffusion-limited crystal growth. Phys Rev B 31(9):6119
23. Curtin WA, Miller RE (2003) Atomistic/continuum coupling in computational materials science. Model Simul Mater Sci Eng 11(3):R33
24. Curtin WA, Miller RE (2017) A perspective on atomistic-continuum multiscale modeling. Model Simul Mater Sci Eng 25(7):071004
25. Danilov D, Nestler B (2004) Dendritic to globular morphology transition in ternary alloy solidification. Phys Rev Lett 93(21):215501
26. Danilov D, Nestler B (2005) Phase-field simulations of solidification in binary and ternary systems using a finite element method. J Cryst Growth 275(1–2):e177–e182
27. Echebarria B, Folch R, Karma A, Plapp M (2004) Quantitative phase-field model of alloy solidification. Phys Rev E 70(6):061604
28. Eiken J, Böttger B, Steinbach I (2006) Multiphase-field approach for multicomponent alloys with extrapolation scheme for numerical application. Phys Rev E 73(6):066122
29. Eiken J, Apel M, Liang SM, Schmid-Fetzer R (2015) Impact of p and sr on solidification sequence and

morphology of hypoeutectic al-si alloys: Combined thermodynamic computation and phase-field simulation. Acta Mater 98:152–163
30. Folch R, Plapp M (2003) Towards a quantitative phase-field model of two-phase solidification. Phys Rev E 68(1):010602
31. Folch R, Plapp M (2005) Quantitative phase-field modeling of two-phase growth. Phys Rev E 72(1):011602
32. Galenko P, Reutzel S, Herlach D, Danilov D, Nestler B (2007) Modelling of dendritic solidification in undercooled dilute ni-zr melts. Acta Mater 55(20):6834–6842
33. Ghosh S, Mukherjee A, Abinandanan T, Bose S (2017) Particles with selective wetting affect spinodal decomposition microstructures. Phys Chem Chem Phys 19(23):15424–15432
34. Ghosh S, Mukherjee A, Arroyave R, Douglas JF (2020) Impact of particle arrays on phase separation composition patterns. J Chem Phys 152(22):224902
35. Gorsse S, Miracle DB, Senkov ON (2017) Mapping the world of complex concentrated alloys. Acta Mater 135:177–187
36. Hoffrogge PW, Mukherjee A, Nani E, Amos PK, Wang F, Schneider D, Nestler B (2021) Multiphase-field model for surface diffusion and attachment kinetics in the grand-potential framework. Phys Rev E 103(3):033307
37. Hohenberg PC, Halperin BI (1977) Theory of dynamic critical phenomena. Rev Mod Phys 49(3):435
38. Horstemeyer MF (2012) Integrated computational materials engineering (ICME) for metals: using multiscale modeling to invigorate engineering design with science. Wiley, Hoboken
39. Hötzer J, Jainta M, Steinmetz P, Nestler B, Dennstedt A, Genau A, Bauer M, Köstler H, Rüde U (2015) Large scale phase-field simulations of directional ternary eutectic solidification. Acta Mater 93:194–204
40. Hötzer J, Steinmetz P, Jainta M, Schulz S, Kellner M, Nestler B, Genau A, Dennstedt A, Bauer M, Köstler H et al (2016) Phase-field simulations of spiral growth during directional ternary eutectic solidification. Acta Mater 106:249–259
41. Hötzer J, Steinmetz P, Dennstedt A, Genau A, Kellner M, Sargin I, Nestler B (2017) Influence of growth velocity variations on the pattern formation during the directional solidification of ternary eutectic al-ag-cu. Acta Mater 136:335–346
42. Hu S, Chen L (2001) A phase-field model for evolving microstructures with strong elastic inhomogeneity. Acta Mater 49(11):1879–1890
43. Huang YL, Bracchi A, Niermann T, Seibt M, Danilov D, Nestler B, Schneider S (2005) Dendritic microstructure in the metallic glass matrix composite zr56ti14nb5cu-7ni6be12. Scr Mater 53(1):93–97
44. Hughes TJ (2012) The finite element method: linear static and dynamic finite element analysis. Courier Corporation, North Chelmsford
45. Jackson KA, Hunt JD (1966) Lamellar and rod eutectic growth. TransMetSocAIME 236(8)
46. Kaka F, Khanna S, Ramamurthy P, Choudhury A (2020) Investigation of process-structure-property relationship in ternary organic photovoltaics. J Appl Phys 128(14):145501
47. Kaka F, Singh RK, Ramamurthy P, Choudhury A (2020) Modeling process-structure-property relationship in organic photovoltaics using a robust diffuse interface approach. AIP Adv 10(6):065304
48. Karma A (2001) Phase-field formulation for quantitative modeling of alloy solidification. Phys Rev Lett 87(11):115701
49. Karma A, Rappel WJ (1996) Phase-field method for computationally efficient modeling of solidification with arbitrary interface kinetics. Phys Rev E 53(4):R3017
50. Karma A, Rappel WJ (1998) Quantitative phase-field modeling of dendritic growth in two and three dimensions. Phys Rev E 57(4):4323
51. Kaxiras E (2003) Atomic and electronic structure of solids. Cambridge University Press, Cambridge
52. Kellner M, Sprenger I, Steinmetz P, Hötzer J, Nestler B, Heilmaier M (2017) Phase-field simulation of the microstructure evolution in the eutectic nial-34cr system. Comput Mater Sci 128:379–387
53. Kellner M, Kunz W, Steinmetz P, Hötzer J, Nestler B (2018) Phase-field study of dynamic velocity variations during directional solidification of eutectic nial-34cr. Comput Mater Sci 145:291–305
54. Kellner M, Hötzer J, Schoof E, Nestler B (2020) Phase-field study of eutectic colony formation in nial-34cr. Acta Mater 182:267–277
55. Kim SG (2007) A phase-field model with antitrapping current for multicomponent alloys with arbitrary thermodynamic properties. Acta Mater 55(13):4391–4399
56. Kim SG, Kim WT, Suzuki T (1998) Interfacial compositions of solid and liquid in a phase-field model with finite interface thickness for isothermal solidification in binary alloys. Phys Rev E 58(3):3316
57. Kim SG, Kim WT, Suzuki T (1999) Phase-field model for binary alloys. Phys Rev E 60(6):7186
58. Kobayashi R (1993) Modeling and numerical simulations of dendritic crystal growth. Phys D 63(3–4):410–423
59. Kumar N (2021) Phd Thesis: co-continuous microstructures through spinodal decomposition in ternary systems: a phase field study. Electronic Thesis and Dissertations of Indian Institute of Science, Bangalore. https://etd.iisc.ac.in/handle/2005/5010
60. Kundin J, Rezende JLL, Emmerich H (2014) Phase-field modeling of the coarsening in multi-component systems. Metall Mater Trans A 45(2):1068–1084
61. Kundin J, Mushongera L, Emmerich H (2015) Phase-field modeling of microstructure formation during

rapid solidification in inconel 718 superalloy. Acta Mater 95:343–356
62. Lahiri A, Choudhury A (2015) Effect of surface energy anisotropy on the stability of growth fronts in multiphase alloys. Trans Indian Inst Met 68(6):1053–1057
63. Lahiri A, Choudhury A (2017) Revisiting Jackson–Hunt calculations: unified theoretical analysis for generic multi-phase growth in a multi-component system. Acta Mater 133:316–332
64. Lahiri A, Choudhury A (2017) Theoretical and numerical investigation of diffusive instabilities in multi-component alloys. J Cryst Growth 459:1–12
65. Lahiri A, Choudhury A (2019) Dendrite tip selection during isothermal free growth in multi-component alloys: marginal stability theories and insights from phase-field simulations. Comput Mater Sci 158:209–218
66. Lahiri A, Abinandanan T, Gururajan M, Bhattacharyya S (2014) Effect of epitaxial strain on phase separation in thin films. Philos Mag Lett 94(11):702–707
67. Lahiri A, Abinandanan T, Choudhury A (2017) Theoretical and numerical study of growth in multi-component alloys. Metall Mater Trans A 48(10):4463–4476
68. Lahiri A, Tiwary C, Chattopadhyay K, Choudhury A (2017) Eutectic colony formation in systems with interfacial energy anisotropy: a phase field study. Comput Mater Sci 130:109–120
69. Langer J (1986) Models of pattern formation in first-order phase transitions. In: Directions in condensed matter physics: memorial volume in Honor of Shang-Keng Ma. World Scientific, pp 165–186
70. Lukas H, Fries S, Sundman B (2007) Computational thermodynamics: the Calphad method. Cambridge University Press, New York
71. Mathis P (2016) Phase-field modelling of solidification microstructures. J Indian Inst Sci 96(3):179–198
72. MICRESS (2019) Micress software. https://micress.rwth-aachen.de/
73. Miracle DB, Senkov ON (2017) A critical review of high entropy alloys and related concepts. Acta Mater 122:448–511
74. Moelans N (2011) A quantitative and thermodynamically consistent phase-field interpolation function for multi-phase systems. Acta Mater 59(3):1077–1086
75. Moelans N, Blanpain B, Wollants P (2008) An introduction to phase-field modeling of microstructure evolution. Calphad 32(2):268–294
76. Mukherjee R, Choudhury A, Nestler B (2013) Composition pathway in fe-cu-ni alloy during coarsening. Model Simul Mater Sci Eng 21(7):075012
77. Nestler B, Choudhury A (2011) Phase-field modeling of multi-component systems. Curr Opin Solid State Mater Sci 15(3):93–105
78. Nestler B, Garcke H, Stinner B (2005) Multicomponent alloy solidification: phase-field modeling and simulations. Phys Rev E 71(4):041609
79. Noubary KD, Kellner M, Steinmetz P, Hoetzer J, Nestler B (2017) Phase-field study on the effects of process and material parameters on the tilt angle during directional solidification of ternary eutectics. Comput Mater Sci 138:403–411
80. Panchal JH, Kalidindi SR, McDowell DL (2013) Key computational modeling issues in integrated computational materials engineering. Comput Aided Des 45(1):4–25
81. Penrose O, Fife PC (1990) Thermodynamically consistent models of phase-field type for the kinetic of phase transitions. Phys D 43(1):44–62
82. Plapp M (2011) Unified derivation of phase-field models for alloy solidification from a grand-potential functional. Phys Rev E 84(3):031601
83. Plapp M, Karma A (2002) Eutectic colony formation: a phase-field study. Phys Rev E 66(6):061608
84. Pusztai T, Rátkai L, Szállás A, Gránásy L (2013) Spiraling eutectic dendrites. Phys Rev E 87(3):032401
85. Ranganathan S (2003) Alloyed pleasures: multimetallic cocktails. Curr Sci 85(10):1404–1406
86. Rátkai L, Szállás A, Pusztai T, Mohri T, Gránásy L (2015) Ternary eutectic dendrites: pattern formation and scaling properties. J Chem Phys 142(15):154501
87. Saunders N, Miodownik AP (1998) CALPHAD (calculation of phase diagrams): a comprehensive guide. Elsevier, New York
88. Sholl D, Steckel JA (2011) Density functional theory: a practical introduction. Wiley, New York
89. Steinbach I (2009) Phase-field models in materials science. Model Simul Mater Sci Eng 17(7):073001
90. Steinbach I (2013) Phase-field model for microstructure evolution at the mesoscopic scale. Annu Rev Mater Res 43:89–107
91. Steinbach I (2013) Why solidification? Why phase-field? JOM 65(9):1096–1102
92. Steinbach I, Pezzolla F (1999) A generalized field method for multiphase transformations using interface fields. Phys D 134(4):385–393
93. Steinbach I, Böttger B, Eiken J, Warnken N, Fries S (2007) Calphad and phase-field modeling: a successful liaison. J Phase Equilib Diffus 28(1):101–106
94. Steinbach I, Zhang L, Plapp M (2012) Phase-field model with finite interface dissipation. Acta Mater 60(6–7):2689–2701
95. Steinmetz P, Hötzer J, Kellner M, Dennstedt A, Nestler B (2016) Large-scale phase-field simulations of ternary eutectic microstructure evolution. Comput Mater Sci 117:205–214
96. Steinmetz P, Kellner M, Hötzer J, Nestler B (2018) Quantitative comparison of ternary eutectic phase-field simulations with analytical 3d Jackson–Hunt approaches. Metall Mater Trans B 49(1):213–224
97. Stinner B, Nestler B, Garcke H (2004) A diffuse interface model for alloys with multiple components and phases. SIAM J Appl Math 64(3):775–799

98. Tadmor EB, Miller RE (2011) Modeling materials: continuum, atomistic and multiscale techniques. Cambridge University Press, Cambridge
99. Tiaden J, Nestler B, Diepers HJ, Steinbach I (1998) The multiphase-field model with an integrated concept for modelling solute diffusion. Phys D 115(1–2):73–86
100. Wang SL, Sekerka R, Wheeler A, Murray B, Coriell S, Braun R, McFadden G (1993) Thermodynamically-consistent phase-field models for solidification. Phys D 69(1–2):189–200
101. Warnken N, Ma D, Drevermann A, Reed RC, Fries S, Steinbach I (2009) Phase-field modelling of as-cast microstructure evolution in nickel-based superalloys. Acta Mater 57(19):5862–5875
102. Wendler F, Mennerich C, Nestler B (2011) A phase-field model for polycrystalline thin film growth. J Cryst Growth 327(1):189–201
103. Wheeler AA, Boettinger WJ, McFadden GB (1992) Phase-field model for isothermal phase transitions in binary alloys. Phys Rev A 45(10):7424
104. Yang C, Xu Q, Liu B (2018) A high precision extrapolation method in multiphase-field model for simulating dendrite growth. J Cryst Growth 490:25–34
105. Zhang L, Steinbach I (2012) Phase-field model with finite interface dissipation: extension to multi-component multi-phase alloys. Acta Mater 60(6–7):2702–2710
106. Zhang L, Stratmann M, Du Y, Sundman B, Steinbach I (2015) Incorporating the calphad sublattice approach of ordering into the phase-field model with finite interface dissipation. Acta Mater 88:156–169
107. Zhu J, Chen LQ, Shen J (2001) Morphological evolution during phase separation and coarsening with strong inhomogeneous elasticity. Model Simul Mater Sci Eng 9(6):499
108. Zienkiewicz OC, Taylor RL, Zhu JZ (2005) The finite element method: its basis and fundamentals. Elsevier, New York

Arka Lahiri is an Assistant Professor in the Metallurgical and Materials Engineering Department, Indian Institute of Technology Roorkee. Prior to this, he was a Post-doc in the Max Planck Institüt für Eisenforschung GmBH, Düsseldorf, Germany. He did his PhD from the Department of Materials Engineering at the Indian Institute of Science (IISc), Bangalore, following his Masters from the same institute. He did his Bachelors in Metallurgy and Materials Engineering from Bengal Engineering and Science University (now known as IIEST), Shibpur. His current research interests involve understanding materials phenomena across different length scales using the computational tools of phase-field modeling, crystal plasticity, and Monte Carlo. He is also interested in using Artificial Intelligence and Machine Learning methods to explore process-structure-property relationships in materials.